Electronic Supplementary Material (ESI) for CrystEngComm.

Sensitive RHEED signature of Ti-excess enabling enhanced cationic composition control during the molecular beam epitaxy of $SrTiO_3$ based solid solutions

Masoumeh Razaghi, Marc d'Esperonnat, Claude Botella, Sébastien Cueff, Romain Bachelet and Guillaume Saint-Girons

Supplementary information

SI1. Detailed procedure used to grow the STO and LSTO/STO heterostructures

The samples considered in the article were grown by solid source MBE on (001)-oriented STO substrates. Before growth, the substrates were annealed under a molecular oxygen partial pressure of $5x10^{-7}$ Torr during 30 min at 700°C and oxide layer growth was then carried out in these conditions, at a growth rate of ~2.5 monolayers (ML)/min, using Knudsen cell for Sr, Ti and La evaporation.

We discuss more specifically here the procedure used to grow the LSTO/STO heterostructure having near stoichiometric composition ([A] ≈ [B] in Fig.3). Similar procedures were used to grow the two other heterostructures, apart from the targeted RHEED pattern considered during LSTO growth. Before growth, the La, Sr and Ti beam equivalent pressures were measured depending on the cell temperatures using a Bayard Alpert gauge. The results of these measurements are depicted in Fig.SI1.

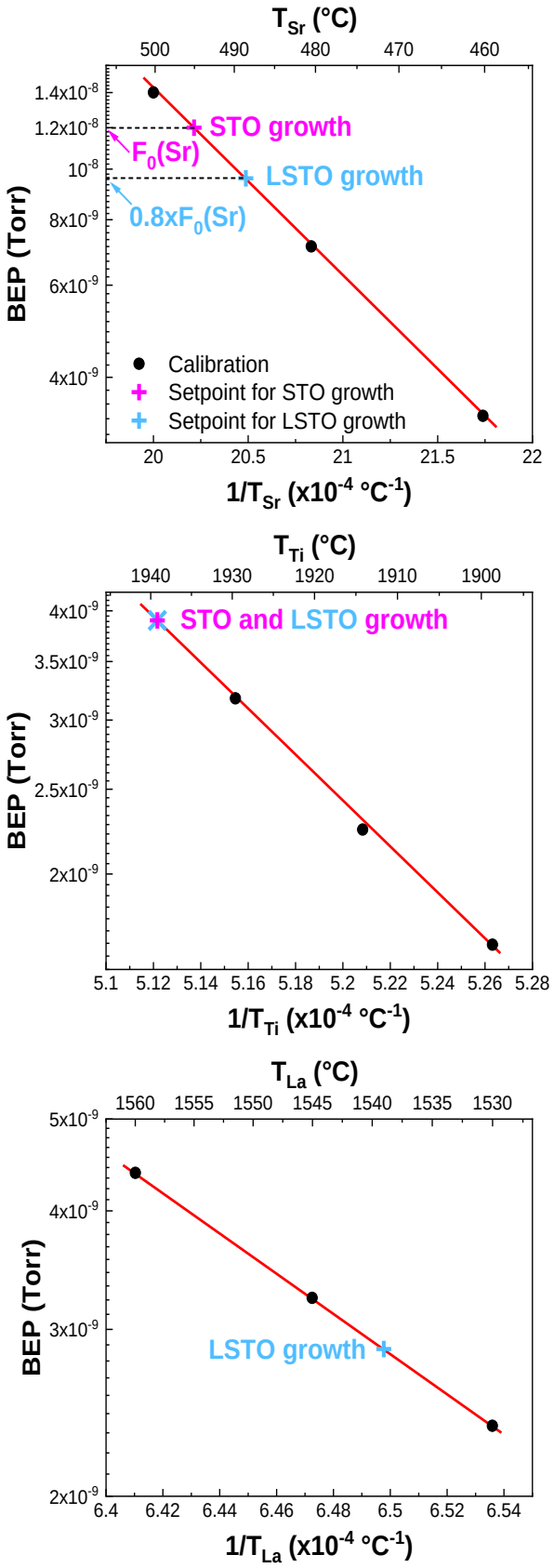

Fig.SI1 *: La, Sr and Ti beam equivalent pressures as a function of the cell temperatures T_{La}, T_{Sr} and T_{Ti}, and setpoints used for STO and LSTO growth*

Then, a STO substrate was introduced in the reactor and prepared as detailed in the main text. For STO growth, the Sr cell temperature was fixed to T_{Sr} = 494.7°C, corresponding to a beam equivalent pressure $F_0(Sr) = 1.2x10^{-8}$ Torr. The Ti cell temperature was tuned during growth to maintain half-order streak free RHEED patterns ([Sr] = [Ti]), leading to a Ti cell temperature T_{Ti} = 1952.5°C (Ti beam equivalent pressure of $3.9x10^{-9}$ Torr). LSTO growth was then carried out by maintaining constant the Ti cell temperature at 1952.5°C, and by tuning the Sr cell temperature to reduce the Sr beam equivalent pressure down to $0.8xF_0(Sr) = 9.6x10^{-9}$ Torr (T_{Sr} = 488.1°C). The growth rate being proportional to the beam equivalent pressure, these growth conditions are expected to correspond to a [Sr]/[Ti] composition ratio of 0.8 in the growing layer, provided that the beam equivalent pressure - Sr cell temperature dependency did not change between calibration and growth. The La cell temperature was tuned during LSTO growth to maintain half-order streak free RHEED patterns along all azimuths (final La cell temperature T_{La} = 1539°C, corresponding to a La beam equivalent pressure of $2.9x10^{-9}$ Torr), which corresponds to a [A]/[B] ratio of 1, as shown in the main text. This means that the ratio ([Sr]+[La])/[Ti] equals unity, and thus that the La atomic substitution rate is 0.2 in LSTO, within the limits discussed in the main text.

SI2. Complete RHEED data

Surface diffraction was monitored during the growth of all samples using RHEED (30 kV e-gun). The RHEED patterns recorded at the end of the growth of all STO samples are shown in Fig.SI2.

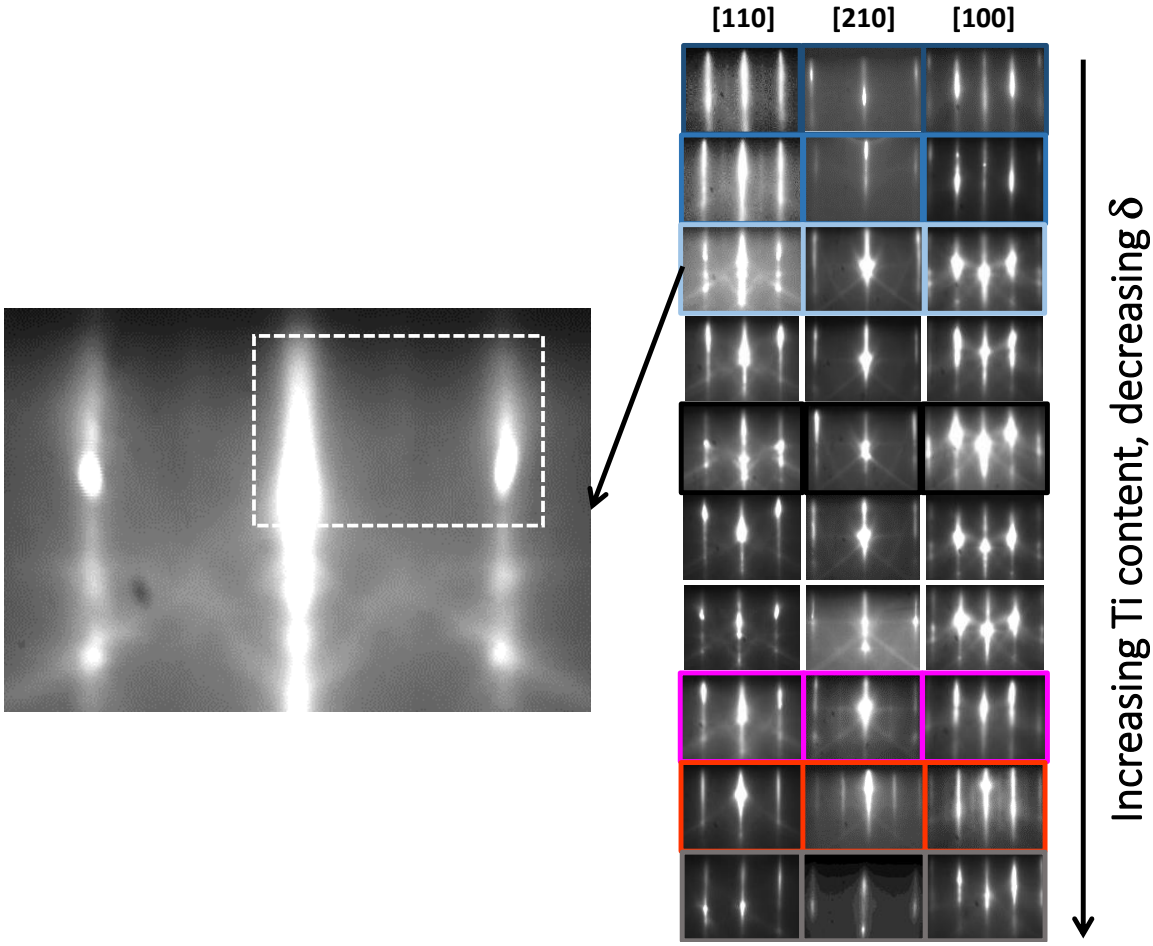

Fig.SI2 *: RHEED patterns recorded at the end of the growth of the STO samples. The frame color code is the same at that used in Fig.2 :* ——, ——, —— *= x2 along the [110] azimuth,* —— *= no reconstruction ($\delta \approx 0$),* —— *= x2 along [210] only,* —— *= x2 along both [210] and [100], and* —— *= no reconstruction on the very Ti-rich surface due to surface disorder. The dotted frame indicate the region of the RHEED selected to be displayed in Fig.2. The profiles shown in Fig.2 are obtained by summing pixel intensities in this region along the vertical direction.*

In this figure, the dotted white frame indicate the region of the patterns displayed in Fig.2 in the main text.

SI3. Composition estimation using XPS

XPS measurements were carried out on the STO samples using an Al-Kα monochromatized X-ray source (hv = 1486.6 eV). Photoelectrons were detected along the normal to the sample surface using a Scienta SES 2002 electron energy analyzer with the X-ray beam impinging at 54° incidence angle (“magical

angle"). The overall resolution was better than 500 meV, and the signal to noise ratio better than 5x10^{-2} in the conditions used for the experiments The XPS spectra of the Sr3d, Ti2p-3/2 and O1s core levels are shown in Fig.SI3, after Shirley background subtraction.

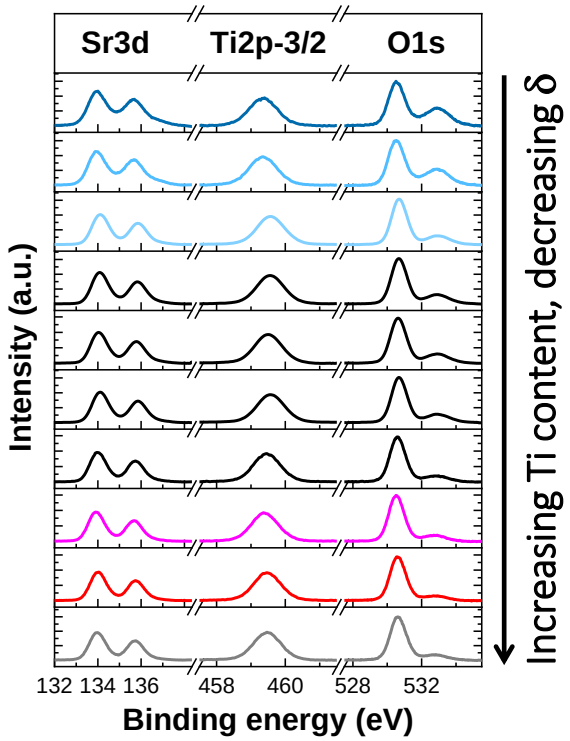

A_{Ti2p}	A_{Sr3d}	A_{Sr3d}/A_{Ti2p}	[Sr]/[Ti]	δ
127972	316651	2.47	1.36	**0.36**
161895	383649	2.37	1.30	**0.30**
156097	307196	1.97	1.08	**0.08**
182310	343279	1.88	1.04	**0.04**
212007	392268	1.85	1.02	**0.02**
177074	318523	1.80	0.99	**-0.01**
265708	462699	1.74	0.96	**-0.04**
263675	454294	1.72	0.95	**-0.05**
285818	469474	1.64	0.90	**-0.1**
251224	385846	1.54	0.84	**-0.16**

Fig.SI3 *: XPS spectra (Sr3d, Ti2p-3/2 and O1s core levels) recorded on the STO samples, after Shirley background subtraction. The color code is the same at that used in Fig.2 : ——, ——, —— = x2 along the [110] azimuth, —— = no reconstruction ($\delta \approx 0$), —— = x2 along [210] only, —— = x2 along both [210] and [100], and —— = no reconstruction on the very Ti-rich surface due to surface disorder. Table : raw areas of the Sr3d (A_{Sr3d}) and Ti2p-3/2 (A_{Ti2p}) core levels, ratio between them (A_{Sr3d}/A_{Ti2p}), ratio between the Sr and Ti atomic compositions in the samples ([Sr]/[Ti]) obtained by normalizing the core level area ratio to the average of that of the samples for which no reconstruction is detected by RHEED (greyed boxes), and δ values ($\delta = \frac{[Sr]}{[Ti]} - 1$).*

The areas of the core level peaks was used to estimate the sample cationic composition, with a relative uncertainty in the ± 2-3% range.[1] For this purpose, with first calculated the ratio between the areas of the Sr3d and Ti2p-3/2 core level peaks for each sample, namely A_{Sr3d}/A_{Ti2p}. Then, we considered the four samples displaying no reconstruction along any azimuth ("no x2" in Eq.SI1, black lines and greyed boxes in Fig.SI3) as nearly stoichiometric, and used as a reference the average value of their A_{Sr3d}/A_{Ti2p} ratios :

$$\left.\frac{A_{Sr3d}}{A_{Ti2p}}\right|_{Ref} = \frac{\sum_{no\times 2}\left(\frac{A_{Sr3d}}{A_{Ti2p}}\right)}{4} \quad .$$ Eq.SI1

Next, the ratio between the Sr and Ti atomic compositions in the samples ([Sr]/[Ti]) was obtained by dividing for each sample the A_{Sr3d}/A_{Ti2p}.ratio by this reference :

$$\frac{[Sr]}{[Ti]} = \frac{\frac{A_{Sr3d}}{A_{Ti2p}}}{\left.\frac{A_{Sr3d}}{A_{Ti2p}}\right|_{Ref}} \quad ,$$ Eq.SI2

and finally, δ was calculated as $\delta = \frac{[Sr]}{[Ti]} - 1$.

SI4. Complete X-ray diffraction data

X-ray experiments were performed using a Rigaku Smartlab diffractometer equipped with a Ge-220 2-bounce monochromator and a 9 kW rotating anode as X-ray source. The results for the STO layers are depicted in Fig.SI4.

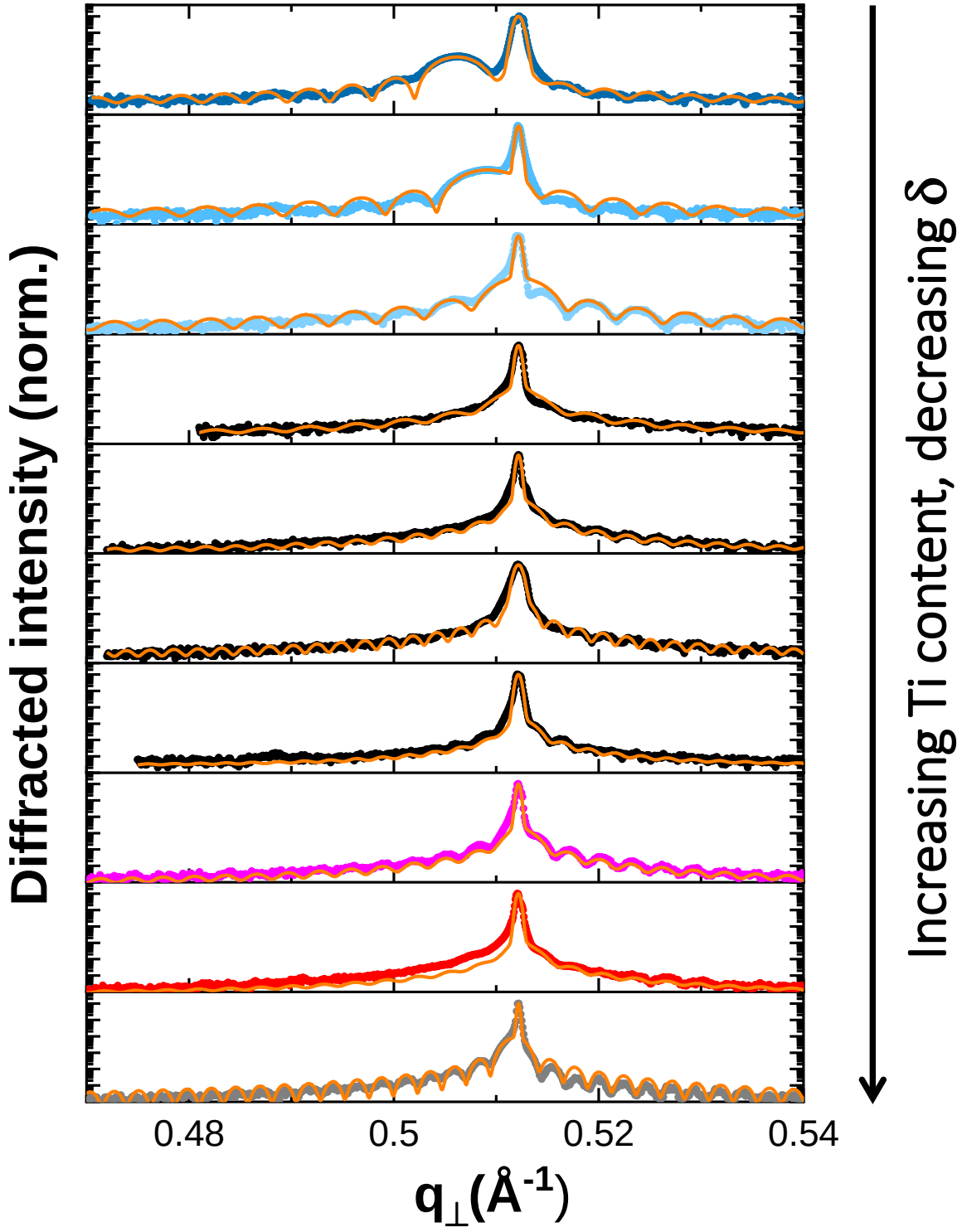

Fig.SI4 *: XRD radial scans recorded around the STO (002) reflection of the STO samples. $q_\perp$ stands for the out-of-plane diffraction vector. The color code is the same at that used in Fig.2 : ——, ——, —— = x2 along the [110] azimuth, —— = no reconstruction ($\delta \approx 0$), —— = x2 along [210] only, —— = x2 along both [210] and [100], and —— = no reconstruction on the very Ti-rich surface due to surface disorder. —— = simulations (kinematic model, perfect (defect-free) layers).*

The diffractograms were fitted using a kinematic model considering perfect (defect free layers).

SI5. Permittivity measurement using spectroscopic ellipsometry

Spectroscopic ellipsometry was used to measure the permittivity of the nearly stoichiometric LSTO/STO heterostructure depending on the incident beam energy E. For this purpose, we used an HORIBA-Jobin Yvon UVISEL Plus ellipsometer enabling measurements ranging from 0.59 to 4.76 eV (0.26 to 2.1 µm). The ellipsometric angles ψ and Δ were measured at four incident angles θ, namely 55, 60, 65 and 70° (Variable Angle Spectroscopic Ellipsometry). The $\psi(E)$ and $\Delta(E)$ functions were fitted (simultaneously for all incidence angles) using convenient oscillator models to extract the complex permittivities ε. In addition, a STO substrate was also analyzed using ellipsometry after an annealing in the MBE reactor simulating the growth of the heterostructure (ie carried out using the same duration and the O_2 partial pressure as that used for sample growth). The STO substrate dielectric function was extracted by ellipsometry, and then injected in the model, in a substrate-layer configuration. The discrepancy between model and experimental data was minimized numerically by minimzing a χ^2 function :

$$\chi^2 = \sum_{E,\theta} \frac{(CalcVal - MeasVal)^2}{\mathrm{MeasVal}} \quad . \qquad \text{Eq.SI3}$$

Perfect match between model and experimental data leads to $\chi^2 = 0$. Fits were performed using the HORIBA-Jobin Yvon DeltaPsi2 software. The best fit was obtained by using an isotropic model combining one Lorentz oscillator, Tauc-Lorentz oscillators and one Drude contribution (for LSTO only).

$$\varepsilon = \varepsilon_\infty + \varepsilon^L + \sum_{j=1}^{n} \varepsilon_j^{TL} + \varepsilon^D, \qquad \text{Eq.SI4}$$

where ε_∞ is the permittivity at infinite frequency, $\varepsilon^L(\omega) = \frac{f \cdot \omega_0^2}{\omega_0^2 - \omega^2 + i \cdot \Gamma_L \cdot \omega}$ (with ω the radiation angular frequency, ω_0 the peak frequency of the oscillator, f the oscillator strength and Γ_L the broadening) is the Lorentz contribution, $\varepsilon_D(\omega) = -\frac{\omega_p^2}{-\omega^2 + i \cdot \Gamma_D \omega}$ (with ω_p the plasma frequency and Γ_D the broadening) is the Drude contribution and $\varepsilon^{TL}(E) = \varepsilon_r^{TL}(E) + i \cdot \varepsilon_i^{TL}(E)$ is the Tauc-Lorentz contribution. The real and imaginary parts of the Tauc-Lorentz contributions read[2]:

$$\varepsilon_i^{TL}(E) = \begin{cases} 0 \; if \; E \le E_g \\ \frac{1}{E} \cdot \frac{A \cdot E_0 \cdot C \cdot (E - E_g)^2}{(E^2 - E_0^2)^2 + C^2 \cdot E^2} \; if \; E > E_g \end{cases}, \text{ and} \qquad \text{Eq.SI5}$$

$$\varepsilon_r^{TL}(E) = \frac{2}{\pi} \int_0^\infty \frac{\chi \cdot \varepsilon_i^{TL}(\chi)}{\chi^2 - E^2} d\chi, \qquad \text{Eq.SI6}$$

where E_g is the optical bandgap of the material, E_0 is the central energy of the transition, A/E_0 its oscillator strength, and C its broadening. This model (without the Drude contribution) is very close to that reported in Ref.3 to describe STO dispersion.

Excellent agreement between experimental and calculated ellipsometric functions was obtained using this procedure, as shown in Fig.SI5.

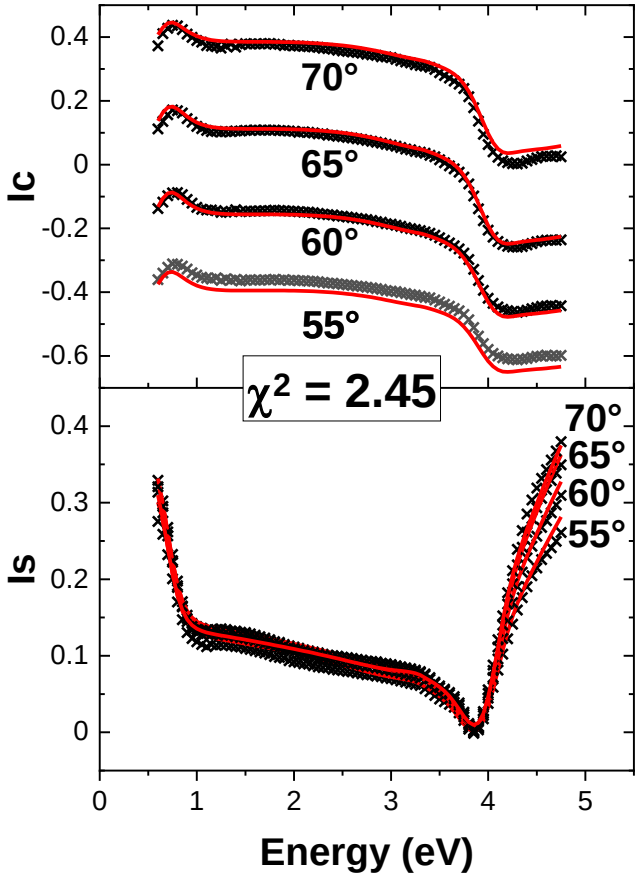

Material		STO	LSTO
E_g		3.22	3.34
ε_∞		1.16	1.61
Tauc-Lorentz 1	A	569	12.65
	E_0	3.85	4.16
	C	1.32	0.57
Tauc-Lorentz 2	A	4.03	122.45
	E_0	4.27	4.67
	C	0.17	2.72
Tauc-Lorentz 3	A	0.59	∅
	E_0	7.51	∅
	C	0.54	∅
Lorentz	f	1.87	0.045
	ω_0	0.71	3.39
	Γ_L	0.80	0.97
Drude	ω_p	∅	**1.38**
	Γ_D	∅	**0.46**

Fig.SI5*: Experimental (crosses) and modeled (solid lines) ellipsometric parameters for the LSTO/STO heterostructure. I_s and I_c are related to the ellipsometric angles ψ and Δ by $I_s = sin(2\psi) \times sin(\Delta)$ and $I_c = sin(2\psi) \times cos(\Delta)$. The low χ^2 value attests for the excellent agreement between calculated and experimental ellipsometric data. The oscillator parameters for STO (both substrate and layer) and STO are given in the table (units = eV except for ε_∞ (unitless))*

In Eq. 1 and 2 of the main text, ω_p is expressed in rad×s^{-1} and Γ_D in s^{-1}, whereas they are expressed in eV in Fig.SI4. The conversion is as follows :

$$\Gamma_D(s^{-1}) = \Gamma_D(eV) \cdot e\frac{2\pi}{h}, \text{ and} \qquad \text{Eq.SI7}$$

$$\omega_p(rad \times s^{-1}) = \omega_p(eV) \cdot e\frac{2\pi}{h}, \qquad \text{Eq.SI8}$$

where e = 1.6×10^{-19} J; and h is the Planck constant.

References

1 R. Hesse, T. Chasse, P. Streubel, and R. Szargan, Surf. Interf. Anal. **36**, 1373 (2004).

2 G.E. Jellison, and F.A. Modine, Appl. Phys. Lett. **69**, 371 (1996).

3 S. Zollner, A.A. Demkov, R. Liu, P.P. Fejes, R.B. Gregory, and P. Alluri, J. Vac. Sci. Technol. B **18**, 2242 (2000).